*Graphical Abstracts (for review)

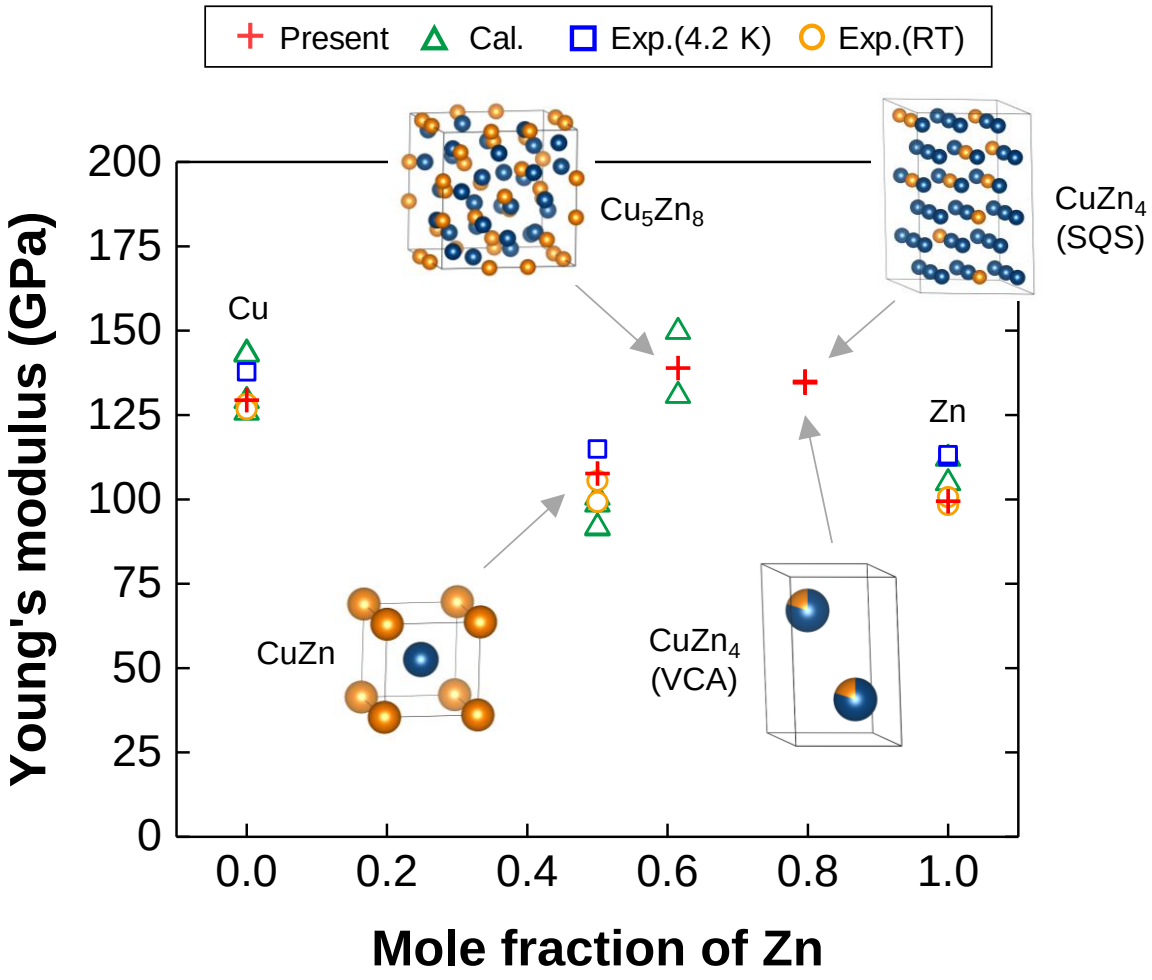

Submitted to Computational Materials Science, December 2019

First-principles calculation of elastic properties of Cu-Zn intermetallic compounds for improving the stiffness of aluminum alloys

Hideaki Iwaoka [a] and Shoichi Hirosawa [a]

[a] Department of Mechanical Engineering and Materials Science, Yokohama National University, 79-5 Tokiwadai, Hodogaya-ku, Yokohama 240-8501, Japan

Keywords:
Intermetallic compound
Young's modulus
Precipitation
First-principles calculation

Abstract

In this study, we computed the elastic properties of Cu-Zn binary intermetallic compounds, CuZn, Cu_5Zn_8 and $CuZn_4$, by first-principles calculation and discussed the capability of the improvement in stiffness of aluminum alloys by aging treatment. The disordered $CuZn_4$ with random atom distribution was emulated for the first time by virtual crystal approximation (VCA) model and special quasirandom structure (SQS) model with symmetry-based projection (SBP) technique. From the present calculation results, it was found that Young's modulus of polycrystalline aggregate of $CuZn_4$ is almost comparable to the highest counterpart of Cu_5Zn_8 with lower elastic anisotropy, but the expected volume fraction of $CuZn_4$ is much higher than that of Cu_5Zn_8 after aging treatment. According to the rule of mixtures for the aluminum matrix and differently oriented intermetallic compounds, therefore, $CuZn_4$ was rationally recommended as the most suitable intermetallic compound for improving the stiffness of Al-Cu-Zn alloys.

1. Introduction

Aging treatment is well known as an effective method to improve the strength of aluminum alloys. Since age-hardening phenomenon was discovered by Wilm in 1906 [1], heat treatment conditions and alloy compositions have been optimized to obtain higher strength, and thus significant expansion of industrial application of aluminum alloys has been accomplished. However, some structural components of industrial products require not only the resistance to plastic

deformation; i.e. strength, but also the resistance to elastic deformation; i.e. stiffness. Unfortunately, the stiffness of aluminum is intrinsically lower than that of other elements (Table 1), and thus commercially compensated by increasing the area or thickness of cross-sectional shapes of the components. Therefore, if the stiffness of aluminum alloys can be improved, application ranges will be further expanded because structural components such as automobile parts have low flexibility in shapes due to limitations of space. To date, temporal changes in Young's modulus during aging treatment have been reported for Al-Cu [4-8], Al-Li [9] and Al-Zn-Mg alloys [8, 10], but none of the high-strength alloys exhibited large enough increase in stiffness from pure aluminum

In general, the stiffness of alloys is represented by elastic moduli such as bulk modulus *B*, shear modulus *G* and Young's modulus *E*, and such elastic moduli are believed to follow the rule of mixtures for the matrix and second phases. Because aging treatment decomposes a supersaturated solid solution into a precipitate microstructure by exploiting the difference of solubility limit, solute elements with larger solubility limit at higher temperatures and smaller solubility limit at lower temperatures become favorable for increasing the volume fraction of the second phase. Copper and zinc satisfy these requirements in aluminum (Table 1), but elastic moduli of Al-Cu or Al-Zn alloy had not been sufficiently improved by aging treatment [4-8, 10]. This is partly attributed to the lower elastic moduli of aluminum-containing intermetallic compounds formed in the two binary systems, and thus in this study we focused on the ternary system, where precipitates comprise only solute elements of Cu and Zn. Note that in the Al-Cu-Zn system CuZn, Cu_5Zn_8 and $CuZn_4$ are expected to precipitate, and thus the most suitable intermetallic compound for improving the stiffness of the ternary alloy can be rationally recommended.

The elastic moduli of intermetallic compounds are measured experimentally, but no elastic properties have been reported for Cu_5Zn_8 and $CuZn_4$. Computational estimation by first-principles calculation is a powerful tool to estimate elastic moduli as well as elastic constant C_{ij} or elastic compliance S_{ij}. The ability to treat not only ordered structures such as CuZn and Cu_5Zn_8 but also disordered structures including $CuZn_4$ is another strength of computational estimation. For example, virtual crystal approximation (VCA) model [11] has been utilized to compute elastic properties of intermetallic compounds with random atom distribution by assuming virtual atoms with intermediate properties in case that the lattice sites are stochastically occupied by two or more kinds of atoms. Although it becomes difficult to compute such an occupation behavior if the elemental atoms are far from each other on the periodic table, our selected copper and zinc are neighboring elements with

similar properties, and thus VCA model becomes applicable to the computation of elastic moduli of disordered $CuZn_4$.

In this study, furthermore, a special quasirandom structure (SQS) model [12] was also employed to emulate random atom distribution in $CuZn_4$. In SQS model, a large supercell composed of several numbers of unit cells is randomly occupied by atoms, and the randomness of the arrangement is evaluated by the correlation function between several atoms arranged into the adjacent lattice sites. The correlation function is then repeatedly renewed in conjunction with the update of the atomic arrangement, resulting in the minimized bias in the arrangement of atoms into the lattice sites. SQS model has been successfully applied to emulate random atom distribution of solid solutions [13, 14] or high-entropy alloys [15, 16], and thus elastic moduli of disordered $CuZn_4$ are expected to be well estimated even in SQS model.

In this study, elastic properties of Cu-Zn binary intermetallic compounds were computed by first-principles calculation. The random atom distribution in $CuZn_4$ was emulated through VCA or SQS model, and the elastic moduli were numerically compared with those of CuZn and Cu_5Zn_8. Based on the present calculation results, furthermore, the most suitable intermetallic compound was rationally recommended for improving the stiffness of Al-Cu-Zn alloy by aging treatment.

2. Computational approach

In this study, elastic properties of pure Cu, pure Zn and three intermetallic compounds of CuZn, Cu_5Zn_8 and $CuZn_4$ were computed by first-principles calculation using Cambridge Sequential Total Energy Package (CASTEP) [17] based on the density functional theory (DFT) and plane-wave pseudopotential method. The reported lattice constants, mass density and elemental atom distribution of these compounds are compared in Table 2 and Fig.1. In VCA model, disordered $CuZn_4$ was emulated by occupying all the lattice sites within its hexagonal close-packed (HCP) structure (c/a = 1.568) by virtual atoms, enabling the properties of zinc with a higher occupation probability of 80% to be strongly reflected by the virtual atoms (Fig.1(c)). In contrast, SQS model was generated using "mcsqs" code [23] of Alloy Theoretic Automated Toolkit (ATAT) [24]. As illustrated in Fig.1(d), eleven Cu atoms and forty-three Zn atoms were first arranged in fifty-four sites of 3×3×3 supercell for $CuZn_4$, and pairs or triplets of atoms with a distance within 1.6*a* (*a* is lattice constant) were selected for evaluating the correlation function between those atoms in SQS model.

The generalized-gradient approximation (GGA) functional of Perdew-Burke-Ernzerhof

(PBE) [25] was utilized as the exchange-correlation term in Kohn-Sham equations, and ultrasoft pseudopotentials [26] were assumed under a condition that cutoff energy of plane-wave is set at 600 eV for Cu, CuZn, Cu_5Zn_8, $CuZn_4$ (VCA) and Zn or at 450 eV for $CuZn_4$ (SQS). The k-point sampling grid in Brillouin zone generated by Monkhorst-Pack scheme [27] was 48×48×48 for Cu (primitive cell), 10×10×10 for CuZn, 8×8×8 for Cu_5Zn_8 (primitive cell), 42×42×24 for $CuZn_4$ (VCA), 4×4×2 for $CuZn_4$ (SQS) and 44×44×20 for Zn respectively. The geometrical optimization was performed using Broyden-Fletcher-Goldfarb-Shanno (BFGS) method [28] in accordance with convergence criteria of 2×10^{-6} eV/atom for energy, 6×10^{-3} eV/Å for maximum force or 2×10^{-4} Å for maximum displacement. The elastic constants were calculated from variations of stress when elastic strain of a maximum magnitude of 3×10^{-3} is applied, whereas the elastic compliances were obtained as inverse matrix of the elastic constants.

3. Results

The lattice constants and mass density of Cu, CuZn, Cu_5Zn_8, $CuZn_4$ and Zn after geometry optimization are listed in Table 2. The difference between the computed and experimentally reported values is within 1%, and thus the present calculation results appear to be correctly estimated. Note that although the lattice constants of $CuZn_4$ (SQS) are slightly deviated from the HCP structure; i.e. $a\neq b$, $\alpha\neq\beta\neq90^{o}$ and $\gamma\neq120^{o}$, the small deviation can be regarded as allowable error for representing the hexagonal structure by SQS model.

The calculated elastic constant C_{ij} and elastic compliance S_{ij} of single crystal of Cu, CuZn, Cu_5Zn_8, $CuZn_4$ and Zn are compared in Table 3 and Table 4 with experimentally reported and previously computed values. It can be seen from Table 3 that C_{ij} of $CuZn_4$ (SQS) does not satisfy the relationship of hexagonal structures;

$$C_{11} = C_{22}, \qquad C_{13} = C_{23}, \qquad C_{44} = C_{55}, \qquad C_{66} = (C_{11} - C_{12})/2 \qquad (1)$$

because the symmetry of crystal structure of $CuZn_4$ is slightly broken after geometry optimization in SQS model. In this study, therefore, we employed a symmetry-based projection (SBP) technique [49, 50] to modify elastic tensor of $CuZn_4$. In SBP technique, elastic tensor is projected to that with a similar but more-symmetric crystal structure, and thus elastic moduli of asymmetrical SQS model can be estimated [14, 16, 51]. The elastic constants calculated from the projected HCP structure, $\bar{C}_{ij}$ [49, 50];

$$\bar{C}_{11} = \frac{3}{8}(C_{11} + C_{22}) + \frac{1}{4}C_{12} + \frac{1}{2}C_{66}, \qquad \bar{C}_{12} = \frac{1}{8}(C_{11} + C_{22}) + \frac{3}{4}C_{12} - \frac{1}{2}C_{66},$$

$$\bar{C}_{13} = \frac{1}{2}(C_{13} + C_{23}), \qquad \bar{C}_{33} = C_{33}, \qquad \bar{C}_{44} = \frac{1}{2}(C_{44} + C_{55}), \qquad (2)$$

are listed in Table 3, whereas the corresponding elastic compliances obtained by inverse matrix calculation of $\bar{C}_{ij}$, $\bar{S}_{ij}$ are listed in Table 4. Note that all the calculation results hereafter were estimated by SQS model with SBP technique.

In general, bulk modulus B and shear modulus G of polycrystalline aggregate are estimated from elastic constant C_{ij} and elastic compliance S_{ij} in Voigt-Reuss-Hill (V-R-H) model [52];

$$B_{\mathrm{V}} = \frac{1}{9}(C_{11} + C_{22} + C_{33}) + \frac{2}{9}(C_{12} + C_{13} + C_{23}), \qquad (3)$$

$$B_{\mathrm{R}} = \frac{1}{(S_{11} + S_{22} + S_{33}) + 2(S_{12} + S_{13} + S_{23})}, \qquad (4)$$

$$G_{\mathrm{V}} = \frac{1}{15}(C_{11} + C_{22} + C_{33}) - \frac{1}{15}(C_{12} + C_{13} + C_{23}) + \frac{1}{5}(C_{44} + C_{55} + C_{66}), \qquad (5)$$

$$G_{\mathrm{R}} = \frac{15}{4(S_{11} + S_{22} + S_{33}) - 4(S_{12} + S_{13} + S_{23}) + 3(S_{44} + S_{55} + S_{66})}, \qquad (6)$$

where subscripts V and R denote Voigt and Reuss models, respectively. In V-R-H model, furthermore, B and G in Hill model, B_{H} and G_{H}, are obtained by taking the average of B or G in Voigt and Reuss models;

$$B_{\mathrm{H}} = \frac{B_{\mathrm{V}} + B_{\mathrm{R}}}{2}, \qquad (7)$$

$$G_{\mathrm{H}} = \frac{G_{\mathrm{V}} + G_{\mathrm{R}}}{2}. \qquad (8)$$

Because Young's modulus E is calculated from B and G by

$$E = \frac{9BG}{3B + G}, \qquad (9)$$

therefore, elastic moduli of polycrystalline aggregate of Cu, CuZn, Cu_5Zn_8, $CuZn_4$ and Zn can be estimated in Table 5. From the fact that elastic moduli of $CuZn_4$ in VCA model and SQS model with SBP technique are close each other, the latter model was confirmed to be another calculation method for emulating random atom distribution in $CuZn_4$. It was also found from Table 5 that in any model E of $CuZn_4$ is almost comparable to the highest E of Cu_5Zn_8, whereas G and E of CuZn significantly differ between Voigt and Reuss models due to the elastic anisotropy of CuZn as described below.

Fig.2 shows the mole fraction dependence of the calculated elastic moduli in Hill model for polycrystalline aggregate of Cu, CuZn, Cu_5Zn_8, $CuZn_4$ and Zn. The present calculation results (red

cross) are compared with literature values of previous computation (green triangle) or experiments (blue square and yellow circle): Cu [29-35], CuZn [29, 36-41], Cu_5Zn_8 [42, 43] and Zn [29, 44-48]. It can be seen from Fig.2 that G_H and E_H possess a non-monotonic variation tendency against mole fraction of Zn, whereas B_H monotonically decreases with increasing Zn content. The similar monotonic tendency of B is reported in other alloy systems [53-55], and attributed to the mass density dependence of B. Because bulk modulus B is defined by pressure P and volume V;

$$B = -V\frac{\partial P}{\partial V}, \qquad (10)$$

therefore, by replacing V by ρ the proportional relationship between B and ρ can be derived. Fig.3 shows the mass density dependence of B_H of polycrystalline aggregate for Cu, CuZn, Cu_5Zn_8, $CuZn_4$ and Zn. As expected, B_H was found to increase linearly with ρ even through the plots of $CuZn_4$ in VCA model and SQS model with SBP technique, confirming again that the latter model is applicable to the emulation of random atom distribution in $CuZn_4$.

Table 6 summarizes the Poisson's ratio ν, Young's modulus to shear modulus ratio in Hill model B/G and universal elastic anisotropy index A_U of Cu, CuZn, Cu_5Zn_8, $CuZn_4$ and Zn. Here, ν was estimated as a ratio of elastic strains generated perpendicular and parallel to applied stress;

$$\nu = \frac{3B - 2G}{6B + 2G}, \qquad (11)$$

whereas A_U was evaluated as a numerical index to represent the degree of elastic anisotropy of single crystals [56];

$$A_U = 5\frac{G_V}{G_R} + \frac{B_V}{B_R} - 6. \qquad (12)$$

Because ν and B/G have been exploited as empirical parameters that determine the fracture morphology of a material; i.e. ductile fracture is likely to occur when $B/G > 1.75$ [57] or $\nu > 0.26$ [58], polycrystalline aggregate of $CuZn_4$ was suggested to be brittle because $CuZn_4$ does not meet these criteria (Table 6). Such embrittlement might be the case if $CuZn_4$ is polycrystalline aggregate, but there will still be a possibility that $CuZn_4$ embedded into aluminum matrix possesses enough ductility available for commercial use. The expected stiffness of those composite aluminum alloys is evaluated and discussed in 4. Discussion.

As for elastic anisotropy, on the other hand, it was found from Table 6 that CuZn has a larger A_U, and thus higher elastic anisotropy than Cu_5Zn_8 and $CuZn_4$ because of its large difference between G_V and G_R (Table 5). This anisotropy can be visually confirmed in Fig.4, where the

magnitude of Young's modulus E in each direction is illustrated not only by color-coding according to each color scale but also by the distance from the center of the three-dimensional (3D) space, using SC-EMA (Self-consistent Calculations of Elasticity of Multi-phase Aggregates) software package [59-61]. Here, E of Cu, CuZn and Cu_5Zn_8 with cubic structures was calculated [62] by

$$\frac{1}{E} = S_{11} - (2S_{11} - 2S_{12} - S_{44})(l_1^2 l_2^2 + l_2^2 l_3^2 + l_3^2 l_1^2)\,, \qquad (13)$$

whereas E of $CuZn_4$ and Zn with hexagonal structures was estimated by

$$\frac{1}{E} = (1 - l_3^2)^2 S_{11} + l_3^4 S_{33} + l_3^2(1 - l_3^2)(2S_{13} + S_{44}) \qquad (14)$$

(l_1, l_2 and l_3 are the directional cosines). It is suggested from "ameboid" shape of the 3D surface in Fig.4(b) that single crystal of CuZn has the highest elastic anisotropy of Young's modulus; i.e. 43.1 GPa, 101.7 GPa and 185.6 GPa in the <100>, <110> and <111> directions, in agreement with the larger elastic anisotropy index A_U (Table 6). In the case of polycrystalline aggregate, however, smaller elastic moduli were inversely estimated for CuZn than those of Cu_5Zn_8 and $CuZn_4$ (Table 5), suggesting that the highest stiffness of optimally aligned grains is averaged out by lower stiffness of the surrounding grains with the different orientations. In the following section, therefore, more elastically isotropic Cu_5Zn_8 and $CuZn_4$ are considered to take advantage of their larger elastic moduli in polycrystalline aggregate (Table 5).

4. Discussion

In this study, elastic properties of Cu-Zn binary intermetallic compounds were computed and compared from the viewpoint of not only the magnitude of elastic moduli but also the elastic anisotropy. The present calculation results revealed that Young's modulus of polycrystalline aggregate of $CuZn_4$ is almost comparable to the highest counterpart of Cu_5Zn_8 (Table 5) with lower elastic anisotropy (Table 6 and Fig.4). Therefore, the improvement in stiffness of aluminum alloys appears to be accomplished by dispersing $CuZn_4$ or Cu_5Zn_8 into the aluminum matrix through aging treatment, because the rule of mixtures consists of Young's moduli of aluminum matrix and differently oriented intermetallic compounds. In this study, the latter was estimated as Young's modulus of polycrystalline aggregate of the compound (Table 5), and thus the expected volume fraction of $CuZn_4$ or Cu_5Zn_8 after aging treatment becomes a determining factor to be investigated.

If it is assumed that Cu_xZn_y is formed from a supersaturated solid solution with a concentration of Al-k Cu- $(y/x)\times k$ Zn (k is atomic fraction) and all solute atoms are used up for the

formation of Cu_xZn_y, the maximum volume of Cu_xZn_y formed from 1 mol of this alloy can be estimated as follows;

$$V_{\mathrm{p}} = \frac{N_{\mathrm{A}} v_{\mathrm{p}} k}{n_{\mathrm{Cu-p}}}, \qquad (15)$$

where $n_{\mathrm{Cu\text{-}p}}$ is the number of Cu atoms in the unit cell of Cu_xZn_y, v_{p} is the volume of the unit cell of Cu_xZn_y and N_{A} is Avogadro number. At this time, the volume of Al matrix can be estimated as follows;

$$V_{\mathrm{Al}} = \frac{N_{\mathrm{A}} v_{\mathrm{Al}} \left(1 - \frac{x+y}{x} k\right)}{n_{\mathrm{Al-Al}}}, \qquad (16)$$

where $n_{\mathrm{Al\text{-}Al}}$ is the number of Al atoms in the unit cell of Al, v_{Al} is the volume of the unit cell of Al. Therefore, the maximum volume fraction of the precipitated intermetallic compound f_{p} can be described as follows;

$$f_{\mathrm{p}} = \frac{n_{\mathrm{Al-Al}} v_{\mathrm{p}} k}{n_{\mathrm{Al-Al}} v_{\mathrm{p}} k + n_{\mathrm{Cu-p}} v_{\mathrm{Al}} \left(1 - \frac{x+y}{x} k\right)}. \qquad (17)$$

This assumption is plausible because solubility limit of copper in aluminum is much lower than that of zinc, allowing f_{p} to be determined only by mole fraction of copper in the supersaturated solid solution. Using $n_{\mathrm{Al\text{-}Al}}$ = 4, $n_{\mathrm{Cu\text{-}p}}(Cu_5Zn_8)$ = 20, $n_{\mathrm{Cu\text{-}p}}(CuZn_4)$ = 0.4, v_{Al} = 66.40 Å^3 and $v_{\mathrm{p}}(Cu_5Zn_8)$ = 699.8 Å^3 and $v_{\mathrm{p}}(CuZn_4)$ = 27.88 Å^3, the maximum volume fraction of the two precipitates were estimated as $f_{\mathrm{p}}(Cu_5Zn_8)$ = 4.26 vol% and $f_{\mathrm{p}}(CuZn_4)$ = 8.53 vol% when k = 2.0 at% in consistent with the fact that smaller mole fraction of copper within $CuZn_4$ can lead to the higher volume fraction of $CuZn_4$ than Cu_5Zn_8.

When two phases are arranged in parallel to or in series to tensile direction, Young's modulus of a composite material consisting of the two phases, E_c, can be described by the following rule of mixtures, respectively [63, 64];

$$E_{\mathrm{c}} = E_1(1 - f_2) + E_2 f_2 \qquad (18)$$

$$\frac{1}{E_{\mathrm{c}}} = \frac{1 - f_2}{E_1} + \frac{f_2}{E_2}, \qquad (19)$$

where the subscripts 1 and 2 denote each phase. The E_{c} values obtained from Eq.(18) and (19) correspond to upper and lower bounds of elastic moduli for the composite material, respectively. Young's modulus of a composite material containing particulate secondary phases takes a value between these bounds. By substituting Young's modulus of aluminum, E(Al) = 70.6 GPa (Table 1), for E_1, and Young's modulus of the precipitated intermetallic compound, $E(Cu_5Zn_8)$ = 138.9 GPa or $E(CuZn_4)$ = 135.0 GPa (Table 5), for E_2, therefore, the increment in Young's modulus from pure

aluminum was found to be 1.5-2.9 GPa by Cu_5Zn_8 or 3.0-5.5 GPa by $CuZn_4$. This indicates that the most suitable intermetallic compound for improving the stiffness of Al-Cu-Zn alloys is high-stiffness but less-anisotropic $CuZn_4$ due to its larger volume fraction after aging treatment. The experimental assessment of the validity of this guideline will be reported elsewhere using a newly developed Al-4wt%Cu-20wt%Zn alloy.

5. Conclusions

The elastic properties of the three Cu-Zn binary intermetallic compounds of CuZn, Cu_5Zn_8 and $CuZn_4$ were computed by first-principles calculations. The random atom distribution of disordered $CuZn_4$ was emulated by virtual crystal approximation (VCA) model and special quasirandom structure (SQS) model with symmetry-based projection (SBP) technique. Based on the present calculation results, the most suitable compound for improving the stiffness of Al-Cu-Zn alloys was recommended as follows.

1. The single crystal of CuZn had higher Young's modulus in a specific direction of <111> than Cu_5Zn_8 and $CuZn_4$. In the case of polycrystalline aggregate, however, smaller elastic moduli were inversely estimated for CuZn, suggesting that the highest stiffness of optimally aligned grains is averaged out by lower stiffness of the surrounding grains with the different orientations.
2. The elastic moduli of disordered $CuZn_4$ were identically computed by VCA model and SQS model with SBP technique, confirming that the latter model is also effective in emulating random atom distribution in $CuZn_4$.
3. Young's modulus of polycrystalline aggregate of $CuZn_4$ was almost comparable to the highest counterpart of Cu_5Zn_8 with lower elastic anisotropy. This suggests that the most suitable intermetallic compound for improving the stiffness of Al-Cu-Zn alloys is high-stiffness but less-anisotropic $CuZn_4$ due to its larger volume fraction after aging treatment.

Acknowledgements

This research was supported by The Light Metals Educational Foundation of Japan. The authors deeply acknowledge the generous support.

References

[1] A. Wilm, Physikalisch-metallurgische Untersuchungen über magnesiumhaltige Aluminiumlegierungen, Metallurgie. 8 (1911) 225–227.

[2] E.A. Brandes, G.B. Brook, Smithells Metals Reference Book, Butterworth -Heinemann, 1992.

[3] J.R. Davis, Aluminum and Aluminum Alloys, ASM International, 1993.

[4] K. Tanaka, H. Abe, K. Hirano, Young's Modulus of Age-Hardend Aluminium Alloys, Nat. Sci. Report, Ochanomizu Univ. 5 (1955) 213–227.

[5] B.J. Elliot, H.J. Axon, The Young's Modulus of Some Quenched and Aged Binary Aluminum Alloys, J. Inst. Met. 86 (1957) 24–28.

[6] C. Chiou, H. Herman, M.E. Fine, Further Studies of GPI Zone Formation in Al-2 At. Pct Cu, Trans. Metall. Soc. AIME. 218 (1960) 299–307.

[7] M. Senoo, T. Hayashi, Elastic Constants of Al-Cu Solid-Solution Alloys and Their Variations by Aging Treatments, JSME Int. J. Ser. I 31 (1988) 664–670.

[8] A. Villuendas, J. Jorba, A. Roca, The Role of Precipitates in the Behavior of Young's Modulus in Aluminum Alloys, Metall. Mater. Trans. A. 45 (2014) 3857–3865.

[9] B. Noble, S.J. Harris, K. Dinsdale, The elastic modulus of aluminium-lithium alloys, J. Mater. Sci. 17 (1982) 461–468.

[10] E. Becker, W. Heyroth, Behaviour of Young's modulus of AlZnMg alloys during homogeneous decomposition, Phys. Status Solidi. (a) 100 (1987) 485–492.

[11] L. Bellaiche, D. Vanderbilt, Virtual crystal approximation revisited: Application to dielectric and piezoelectric properties of perovskites, Phys. Rev. B. 61 (2000) 7877–7882.

[12] A. Zunger, S. Wei, L.G. Ferreira, J.E. Bernard, Special quasirandom structures, Phys. Rev. Lett. 65 (1990) 353–356.

[13] W. Zhou, R. Sahara, K. Tsuchiya, First-principles study of the phase stability and elastic properties of Ti-X alloys (X = Mo, Nb, Al, Sn, Zr, Fe, Co, and O), J. Alloys Compd. 727 (2017) 579–595.

[14] C. Marker, S.L. Shang, J.C. Zhao, Z.K. Liu, Effects of alloying elements on the elastic properties of bcc Ti-X alloys from first-principles calculations, Comput. Mater. Sci. 142 (2018) 215–226.

[15] A.J. Zaddach, C. Niu, C.C. Koch, D.L. Irving, Mechanical properties and stacking fault energies of NiFeCrCoMn high-entropy alloy, JOM. 65 (2013) 1780–1789.

[16] F. Tian, Y. Wang, L. Vitos, Impact of aluminum doping on the thermo-physical properties of

refractory medium-entropy alloys, J. Appl. Phys. 121 (2017) 015105.

[17] M.D. Segall, P.J.D. Lindan, M.J. Probert, C.J. Pickard, P.J. Hasnip, S.J. Clark, M.C. Payne, First-principles simulation : ideas, illustrations and the CASTEP code, J. Phys. Condens. Matter. 14 (2002) 2717–2744.

[18] M.E. Straumanis, L.S. Yu, Lattice parameters, densities, expansion coefficients and perfection of structure of Cu and of Cu–In α phase, Acta Crystallogr. A25 (1969) 676–682.

[19] S.S. Rao, T.R. Anantharaman, Constitution of brasses below 500℃, Z. Metallkd. 60 (1969) 312–315.

[20] J.K. Brandon, R.Y. Brizard, P.C. Chieh, R.K. McMillan, W.B. Pearson, New Refinements of the γ brass Type Structures Cu_5Zn_8, Cu_5Cd_8 and Fe_3Zn_{10}, Acta Crystallogr. B30 (1974) 1412–1417.

[21] T.B. Massalski, H.W. King, The lattice spacing relationships in H.C.P. ε and η phases in the systems Cu-Zn, Ag-Zn, Au-Zn and Ag-Cd, Acta Metall. 10 (1962) 1171–1181.

[22] J.R. Brown, The Solid Solution of Cadmium in Zinc, J. Inst. Met. 83 (1954) 49–52.

[23] A. Van De Walle, P. Tiwary, M. De Jong, D.L. Olmsted, M. Asta, A. Dick, D. Shin, Y. Wang, L.Q. Chen, Z.K. Liu, Efficient stochastic generation of special quasirandom structures, Calphad Comput. Coupling Phase Diagrams Thermochem. 42 (2013) 13–18.

[24] A. van de Walle, G. Ceder, Automating first-principles phase diagram calculations, J. Phase Equilibria. 23 (2002) 348–359.

[25] J.P. Perdew, K. Burke, M. Ernzerhof, Generalized Gradient Approximation Made Simple, Phys. Rev. Lett. 77 (1996) 3865–3868.

[26] D. Vanderbilt, Soft self-consistent pseudopotentials in a generalized eigenvalue formalism, Phys. Rev. B. 41 (1990) 7892–7895.

[27] H.J. Monkhorst, J.D. Pack, Special points for Brillouin-zone integrations, Phys. Rev. B. 13 (1976) 5188–5192.

[28] B.G. Pfrommer, M. Côté, S.G. Louie, M.L. Cohen, Relaxation of Crystals with the Quasi-Newton Method, J. Comput. Phys. 131 (1997) 233–240.

[29] L. Cheng, Z. Shuai, Z. Yu, Z. Da-Wei, H. Chao-Zheng, L. Zhi-Wen, Insights into structural and thermodynamic properties of the intermetallic compound in ternary Mg-Zn-Cu alloy under high pressure and high temperature, J. Alloys Compd. 597 (2014) 119–123.

[30] W. Zhou, L. Liu, B. Li, Q. Song, P. Wu, Structural, Elastic, and Electronic Properties of Al-Cu Intermetallics from First-Principles Calculations, J. Electron. Mater. 38 (2009) 356–364.

[31] G. Ghosh, First-principles calculations of structural energetics of Cu–TM (TM = Ti , Zr , Hf) intermetallics, Acta Mater. 55 (2007) 3347–3374.

[32] C. Bercegeay, S. Bernard, First-principles equations of state and elastic properties of seven metals, Phys. Rev. B72 (2005) 214101.

[33] W.C. Overton, J. Gaffney, Temperature Variation of the Elastic Constants of Cubic Elements. I. Copper, Phys. Rev. 98 (1955) 969–977.

[34] Y.A. Chang, L. Himmel, Temperature Dependence of the Elastic Constants of Cu, Ag, and Au above Room Temperature, J. Appl. Phys. 37 (1966) 3567–3572.

[35] R.E. Schmunk, C.S. Smith, Elastic constants of copper-nickel alloys, Acta Metall. 8 (1960) 396–401.

[36] O. Alsalmi, M. Sanati, R.C. Albers, T. Lookman, A. Saxena, First-principles study of phase stability of bcc XZn (X = Cu, Ag, and Au) alloys, Phys. Rev. Mater. 2 (2018) 113601.

[37] R. Sun, D.D. Johnson, Stability maps to predict anomalous ductility in B2 materials, Phys. Rev. B. 87 (2013) 104107.

[38] X.F. Wang, T.E. Jones, W. Li, Y.C. Zhou, Extreme Poisson's ratios and their electronic origin in B2 CsCl-type AB intermetallic compounds, Phys. Rev. B. 85 (2012) 134108.

[39] G.M. McManus, Elastic Properties of β-CuZn, Phys. Rev. 129 (1963) 2004–2007.

[40] Y. Murakami, S. Kachi, Lattice Softening and Phase Stability of CuZn, AgZn and AuZn β Phase Alloys, Jpn. J. Appl. Phys. 13 (1974) 1728–1732.

[41] P.L. Young, A. Bienenstock, Elastic Constants of β-Brass from Room Temperature to Above 520℃, J. Appl. Phys. 42 (1971) 3008–3009.

[42] L. Yang, W. Jiong, G. Qian-nan, D. Yong, Structural, elastic and electronic properties of Cu-X compounds from first-principles calculations, J. Cent. South Univ. 22 (2015) 1585–1594.

[43] W. Zhou, L. Liu, P. Wu, Structural, electronic and thermo-elastic properties of Cu_6Sn_5 and Cu_5Zn_8 intermetallic compounds: First-principles investigation, Intermetallics. 18 (2010) 922–928.

[44] W.C. Hu, Y. Liu, D.J. Li, H.L. Jin, Y.X. Xu, C.S. Xu, X.Q. Zeng, Structural, anisotropic elastic and electronic properties of Sr-Zn binary system intermetallic compounds: A first-principles study, Comput. Mater. Sci. 99 (2015) 381–389.

[45] G.A. Alers, J.R. Neighbours, The elastic constants of zinc between 4.2° and 670°K, J. Phys. Chem. Solids. 7 (1958) 58–64.

[46] C.W. Garland, R. Dalven, Elastic Constants of Zinc from 4.2°K to 77.6°K, Phys. Rev. 111

(1958) 1232–1234.

[47] C.A. Wert, E.P.T. Tyndall, Elasticity of Zinc Crystals, J. Appl. Phys. 20 (1949) 587–589.

[48] P.W. Bridgman, Some Properties of Single Metal Crystals, Proc. Natl. Acad. Sci. U.S.A. 10 (1924) 411–415.

[49] J.T. Browaeys, S. Chevrot, Decomposition of the elastic tensor and geophysical applications, Geophys. J. Int. 159 (2004) 667–678.

[50] M. Moakher, A.N. Norris, The closest elastic tensor of arbitrary symmetry to an elasticity tensor of lower symmetry, J. Elast. 85 (2006) 215–263.

[51] F. Tasnádi, M. Odén, I.A. Abrikosov, Ab initio elastic tensor of cubic $Ti_{0.5}Al_{0.5}N$ alloys: Dependence of elastic constants on size and shape of the supercell model and their convergence, Phys. Rev. B 85 (2012) 144112.

[52] R. Hill, The Elastic Behaviour of a Crystalline Aggregate, Proc. Phys. Soc. A65 (1952) 349–354.

[53] B. Wen, J. Zhao, F. Bai, T. Li, First-principle studies of Al-Ru intermetallic compounds, Intermetallics. 16 (2008) 333–339.

[54] J. Du, B. Wen, R. Melnik, Y. Kawazoe, Phase stability , elastic and electronic properties of Cu–Zr binary system intermetallic compounds: A first-principles study, J. Alloys Compd. 588 (2014) 96–102.

[55] J. Du, B. Wen, R. Melnik, Y. Kawazoe, First-principles studies on structural, mechanical, thermodynamic and electronic properties of Ni-Zr intermetallic compounds, Intermetallics. 54 (2014) 110–119.

[56] S.I. Ranganathan, M. Ostoja-Starzewski, Universal Elastic Anisotropy Index, Phys. Rev. Lett. 101 (2008) 055504.

[57] S.F. Pugh, Relations between the elastic moduli and the plastic properties of polycrystalline pure metals, London, Edinburgh, Dublin Philos. Mag. J. Sci. 45 (1954) 823–843.

[58] J.J. Lewandowski, W.H. Wang, A.L. Greer, Intrinsic plasticity or brittleness of metallic glasses, Philos. Mag. Lett. 85 (2005) 77–87.

[59] H. Titrian, U. Aydin, M. Friák, D. Ma, D. Raabe, J. Neugebauer, Self-consistent Scale-bridging Approach to Compute the Elasticity of Multi-phase Polycrystalline Materials, Mater. Res. Soc. Symp. Proc. 1524 (2013) mrsf12-1524-rr06-03.

[60] M. Friák, W.A. Counts, D. Ma, B. Sander, D. Holec, D. Raabe, J. Neugebauer, Theory-Guided

Materials Design of Multi-Phase Ti-Nb Alloys with Bone-Matching Elastic Properties, Materials 5 (2012) 1853–1872.

[61] L.F. Zhu, M. Friák, L. Lymperakis, H. Titrian, U. Aydin, A.M. Janus, H.O. Fabritius, A. Ziegler, S. Nikolov, P. Hemzalová, D. Raabe, J. Neugebauer, Ab initio study of single-crystalline and polycrystalline elastic properties of Mg-substituted calcite crystals, J. Mech. Behav. Biomed. Mater. 20 (2013) 296–304.

[62] L.A. Shuvalov, Modern Crystallography IV (Physical Properties of Crystals), Springer, 1988.

[63] W. Voigt, Ueber die Beziehung zwischen den beiden Elasticitätsconstanten isotroper Körper, Ann. Phys. 274 (1889) 573–587.

[64] A. Reuss, Berechnung der Fließgrenze von Mischkristallen auf Grund der Plastizitätsbedingung für Einkristalle, Z. Angew. Math. Und Mech. 9 (1929) 49–58.

Captions

Table 1 Young's modulus of polycrystalline aggregate of Al, Cu, Zn and Fe at room temperature, E_{poly} and maximum solubility limit of Cu, Zn and Fe in Al, *S*.

Table 2 Lattice constants *a*, *b*, *c*, α, β, γ and mass density ρ of Cu, CuZn, Cu_5Zn_8, $CuZn_4$ and Zn. The present calculation results are compared with experimentally reported values.

Table 3 Elastic constants C_{ij} of single crystal of Cu, CuZn, Cu_5Zn_8, $CuZn_4$ and Zn. The present calculation results are compared with experimentally reported and previously computed values.

Table 4 Elastic compliances S_{ij} of single crystal of Cu, CuZn, Cu_5Zn_8, $CuZn_4$ and Zn. The present calculation results are compared with experimentally reported and previously computed values.

Table 5 Bulk modulus B_{poly}, shear modulus G_{poly} and Young's modulus E_{poly} of polycrystalline aggregate of Cu, CuZn, Cu_5Zn_8, $CuZn_4$ and Zn. The present calculation results in Voigt, Reuss and Hill models are compared with experimentally reported and previously computed values.

Table 6 Poisson's ratio *v*, bulk modulus to shear modulus ratio B_H/G_H and universal elastic anisotropy index A_U of Cu, CuZn, Cu_5Zn_8, $CuZn_4$ and Zn. The present calculation results are compared with experimentally reported and previously computed values.

Fig.1 Elemental atom distribution of (a) CuZn, (b) Cu_5Zn_8 and $CuZn_4$ in (c) VCA model or (d) SQS (3×3×3 supercell) model before geometry optimization.

Fig.2 Mole fraction dependence of (a) bulk modulus B_H, (b) shear modulus G_H and (c) Young's modulus E_H of polycrystalline aggregate for Cu, CuZn, Cu_5Zn_8, $CuZn_4$ and Zn. The present calculation results in Hill model are compared with experimentally reported and previously computed values.

Fig.3 Mass density dependence of bulk modulus B_H of polycrystalline aggregate for Cu, CuZn, Cu_5Zn_8, $CuZn_4$ and Zn. The present calculation results in Hill model are compared with experimentally reported and previously computed values.

Fig.4 Directional anisotropy of Young's modulus *E* of single crystal for Cu, CuZn, Cu_5Zn_8, $CuZn_4$ and Zn. The magnitude of *E* in each direction is illustrated not only by color-coding according to each color scale but also by the distance from the center of the three-dimensional space.

Table

Table 1 Young's modulus of polycrystalline aggregate of Al, Cu, Zn and Fe at room temperature, E_{poly} and maximum solubility limit of Cu, Zn and Fe in Al, S.

	E_{poly} (GPa) [2]	S (at%) [3]
Al	70.6	
Cu	129.8	2.48
Zn	104.5	66.4
Fe	211.4	0.025

Table 2 Lattice constants *a, b, c, α, β, γ* and mass density *ρ* of Cu, CuZn, Cu_5Zn_8, $CuZn_4$ and Zn. The present calculation results are compared with experimentally reported values.

Phase Space group		***a*** **(Å)**	***b*** **(Å)**	***c*** **(Å)**	**α (deg.)**	**β (deg.)**	**γ (deg.)**	***ρ*** **(g/cm³)**	
Cu *Fm-3m (225)*	Present	3.630	-	-	-	-	-	8.824	
	Exp.	3.615	-	-	-	-	-	8.935	[18]
CuZn *Pm-3m (221)*	Present	2.959	-	-	-	-	-	8.264	
	Exp.	2.958	-	-	-	-	-	8.270	[19]
Cu_5Zn_8 *I-43m (217)*	Present	8.858	-	-	-	-	-	8.035	
	Exp.	8.878	-	-	-	-	-	7.981	[20]
$CuZn_4$ *$P6_3/mmc$ (194)*	Present(VCA)	2.747	-	4.291	-	-	-	7.702	
	Present(SQS)	2.744	2.748	4.291	90.00	90.01	120.99	7.782	
	Exp.	2.738	-	4.294	-	-	-	7.744	[21]
Zn *$P6_3/mmc$ (194)*	Present	2.640	-	4.977	-	-	-	7.231	
	Exp.	2.665	-	4.947	-	-	-	7.138	[22]

Table 3 Elastic constants C_{ij} of single crystal of Cu, CuZn, Cu_5Zn_8, $CuZn_4$ and Zn. The present calculation results are compared with experimentally reported and previously computed values.

		Elastic constant of single crystal (GPa)									
		C_{11}	C_{12}	C_{13}	C_{22}	C_{23}	C_{33}	C_{44}	C_{55}	C_{66}	
Cu	Present	170.8	121.5					75.3			
	Cal.	176.0	118.2					81.9			[29]
	Cal.	183.5	125.9					80.9			[30]
	Cal.	171.2	123.1					72.4			[31]
	Cal.	171.1	122.2					75.3			[32]
	Exp. at 4.2 K	176.2	124.9					81.8			[33]
	Exp. at RT	170.0	122.5					75.8			[34]
	Exp. at RT	168.1	121.5					75.1			[35]
CuZn	Present	134.8	104.7					75.4			
	Cal.	126.3	110.5					89.3			[36]
	Cal.	130.2	112.5					83.1			[29]
	Cal.	124.0	108.7					78.6			[37]
	Cal.	123.4	110.9					84.3			[38]
	Exp. at 4.2 K	139.6	109.2					82.3			[39]
	Exp. at RT	131.1	101.5					73.8			[40]
	Exp. at RT	127.1	107.1					80.3			[41]
Cu_5Zn_8	Present	204.3	59.7					44.4			
	Cal.	195.6	61.5					41.7			[42]
	Cal.	185.3	72.9					60.5			[43]
$CuZn_4$	Present(VCA)	149.4	52.4	57.9			182.2	58.7			
	Present(SQS)	157.9	49.8	63.8	148.0	63.7	170.3	76.0	63.8	35.9	
	Present (SQS+SBP)	145.1	57.7	63.7			170.3	69.9			
Zn	Present	175.5	43.2	51.2			58.7	36.1			
	Cal.	170.7	29.8	40.4			61.3	44.6			[44]
	Cal.	171.0	37.3	51.9			63.7	41.3			[29]
	Exp. at 4.2 K	179.1	37.5	55.4			68.8	46.0			[45]
	Exp. at 4.2 K	177.0	34.8	52.8			68.5	45.9			[46]
	Exp. at RT	160.9	33.5	50.1			61.0	38.3			[47]
	Exp. at RT	159.0	32.3	48.2			62.1	40.0			[48]

Table 4 Elastic compliances S_{ij} of single crystal of Cu, CuZn, Cu_5Zn_8, $CuZn_4$ and Zn. The present calculation results are compared with experimentally reported and previously computed values.

		Elastic compliance of single crystal (TPa^{-1})									
		S_{11}	S_{12}	S_{13}	S_{22}	S_{23}	S_{33}	S_{44}	S_{55}	S_{66}	
Cu	Present	14.35	-5.97					13.29			
	Cal.	12.33	-4.95					12.20			[29]
	Cal.	12.34	-5.02					12.36			[30]
	Cal.	14.65	-6.13					13.82			[31]
	Cal.	14.44	-6.01					13.28			[32]
	Exp. at 4.2 K	13.78	-5.72					12.22			[33]
	Exp. at RT	14.84	-6.21					13.19			[34]
	Exp. at RT	15.12	-6.34					13.31			[35]
CuZn	Present	23.18	-10.14					13.26			
	Cal.	43.15	-20.14					11.20			[36]
	Cal.	38.75	-17.97					12.04			[29]
	Cal.	44.55	-20.81					12.72			[37]
	Cal.	54.30	-25.70					11.86			[38]
	Exp. at 4.2 K	22.86	-10.03					12.15			[39]
	Exp. at RT	23.52	-10.26					13.55			[40]
	Exp. at RT	34.31	-15.69					12.45			[41]
Cu_5Zn_8	Present	5.64	-1.28					22.51			
	Cal.	6.02	-1.44					23.98			[42]
	Cal.	6.94	-1.96					16.53			[43]
$CuZn_4$	Present(VCA)	8.19	-2.12	-1.93			6.72	17.04			
	Present(SQS)	8.19	-2.33	-2.15	9.61	-2.80	7.74	13.52	16.10	32.59	
	Present (SQS+SBP)	8.94	-2.49	-2.41			7.68	14.31			
Zn	Present	7.64	0.08	-6.74			28.80	27.74			
	Cal.	6.95	-0.15	-4.48			22.22	22.41			[44]
	Cal.	7.79	0.31	-6.60			26.47	24.21			[29]
	Exp. at 4.2 K	7.46	0.39	-6.32			24.72	21.76			[45]
	Exp. at 4.2 K	7.35	0.32	-5.92			23.72	21.79			[46]
	Exp. at RT	8.38	0.54	-7.33			28.43	26.11			[47]
	Exp. at RT	8.24	0.35	-6.66			26.45	25.00			[48]

Table 5 Bulk modulus B_{poly}, shear modulus G_{poly} and Young's modulus E_{poly} of polycrystalline aggregate of Cu, CuZn, Cu_5Zn_8, $CuZn_4$ and Zn. The present calculation results in Voigt, Reuss and Hill models are compared with experimentally reported and previously computed values.

		B_{poly} (GPa)			G_{poly} (GPa)			E_{poly} (GPa)			
		B_V	B_R	B_H	G_V	G_R	G_H	E_V	E_R	E_H	
Cu	Present	137.9	137.9	137.9	55.0	41.3	48.1	145.7	112.6	129.4	
	Cal.	137.4	137.4	137.4	60.7	47.3	54.0	158.8	127.3	143.3	[29]
	Cal.	145.1	145.1	145.1	60.1	46.9	53.5	158.3	127.1	142.9	[30]
	Cal.	139.1	139.1	139.1	53.0	40.1	46.6	141.2	109.9	125.7	[31]
	Cal.	138.5	138.5	138.5	55.0	41.1	48.0	145.6	112.2	129.2	[32]
	Exp. at 4.2 K	142.0	142.0	142.0	59.3	43.6	51.5	156.3	118.7	137.8	[33]
	Exp. at RT	138.3	138.3	138.3	55.0	40.4	47.7	145.6	110.4	128.3	[34]
	Exp. at RT	137.0	137.0	137.0	54.4	39.8	47.1	144.1	108.7	126.7	[35]
CuZn	Present	114.7	114.7	114.7	51.3	28.9	40.1	133.8	80.0	107.7	
	Cal.	115.8	115.8	115.8	56.7	17.4	37.1	146.3	49.8	100.5	[36]
	Cal.	118.4	118.4	118.4	53.4	19.0	36.2	139.2	54.1	98.5	[29]
	Cal.	113.8	113.8	113.8	50.2	16.7	33.5	131.3	47.7	91.4	[37]
	Cal.	115.1	115.1	115.1	53.1	14.1	33.6	138.0	40.5	91.8	[38]
	Exp. at 4.2 K	119.3	119.3	119.3	55.5	29.8	42.6	144.1	82.4	114.2	[39]
	Exp. at RT	111.4	111.4	111.4	50.2	28.4	39.3	130.9	78.6	105.5	[40]
	Exp. at RT	113.8	113.8	113.8	52.2	21.1	36.6	135.8	59.5	99.2	[41]
Cu_5Zn_8	Present	107.9	107.9	107.9	55.6	52.5	54.0	142.3	135.6	138.9	
	Cal.	106.2	106.2	106.2	51.8	49.1	50.5	133.8	127.7	130.7	[42]
	Cal.	110.4	110.4	110.4	58.8	58.7	58.7	149.8	149.6	149.7	[43]
$CuZn_4$	Present(VCA)	90.8	89.8	90.3	54.0	53.5	53.8	135.2	133.9	134.6	
	Present (SQS+SBP)	92.3	91.6	91.9	55.1	52.4	53.8	137.8	132.1	135.0	
Zn	Present	77.9	57.8	67.8	45.2	34.0	39.6	113.7	85.2	99.4	
	Cal.	69.3	55.9	62.6	51.4	41.9	46.7	123.6	100.6	112.1	[44]
	Cal.	76.4	61.5	69.0	47.5	36.6	42.1	118.1	91.6	104.9	[29]
	Exp. at 4.2 K	80.4	66.1	73.2	51.1	39.4	45.3	126.5	98.7	112.6	[45]
	Exp. at 4.2 K	78.1	64.9	71.5	51.4	40.2	45.8	126.4	100.1	113.2	[46]
	Exp. at RT	72.2	59.0	65.6	44.7	34.0	39.3	111.1	85.6	98.4	[47]
	Exp. at RT	70.8	59.0	64.9	45.4	35.6	40.5	112.3	89.0	100.6	[48]

Table 6 Poisson's ratio v, bulk modulus to shear modulus ratio B_H/G_H and universal elastic anisotropy index A_U of Cu, CuZn, Cu_5Zn_8, $CuZn_4$ and Zn. The present calculation results are compared with experimentally reported and previously computed values.

		v	B_H/G_H	A_U	
Cu	Present	0.34	2.87	1.66	
	Cal.	0.33	2.54	1.42	[29]
	Cal.	0.34	2.71	1.40	[30]
	Cal.	0.35	2.99	1.61	[31]
	Cal.	0.34	2.88	1.69	[32]
	Exp. at 4.2 K	0.34	2.76	1.80	[33]
	Exp. at RT	0.35	2.90	1.81	[34]
	Exp. at RT	0.35	2.91	1.84	[35]
CuZn	Present	0.34	2.86	3.87	
	Cal.	0.36	3.26	11.27	[36]
	Cal.	0.36	3.27	9.03	[29]
	Cal.	0.37	3.40	10.05	[37]
	Cal.	0.37	3.43	13.87	[38]
	Exp. at 4.2 K	0.34	2.80	4.32	[39]
	Exp. at RT	0.34	2.83	3.82	[40]
	Exp. at RT	0.35	3.11	7.39	[41]
Cu_5Zn_8	Present	0.29	2.00	0.29	
	Cal.	0.29	2.10	0.28	[42]
	Cal.	0.27	1.88	0.01	[43]
$CuZn_4$	Present (VCA)	0.25	1.68	0.06	
	Present (SQS+SBP)	0.26	1.71	0.26	
Zn	Present	0.26	1.71	2.01	
	Cal.	0.20	1.34	1.37	[44]
	Cal.	0.25	1.64	1.74	[29]
	Exp. at 4.2 K	0.24	1.62	1.70	[45]
	Exp. at 4.2 K	0.24	1.56	1.59	[46]
	Exp. at RT	0.25	1.67	1.79	[47]
	Exp. at RT	0.24	1.60	1.58	[48]

Figure

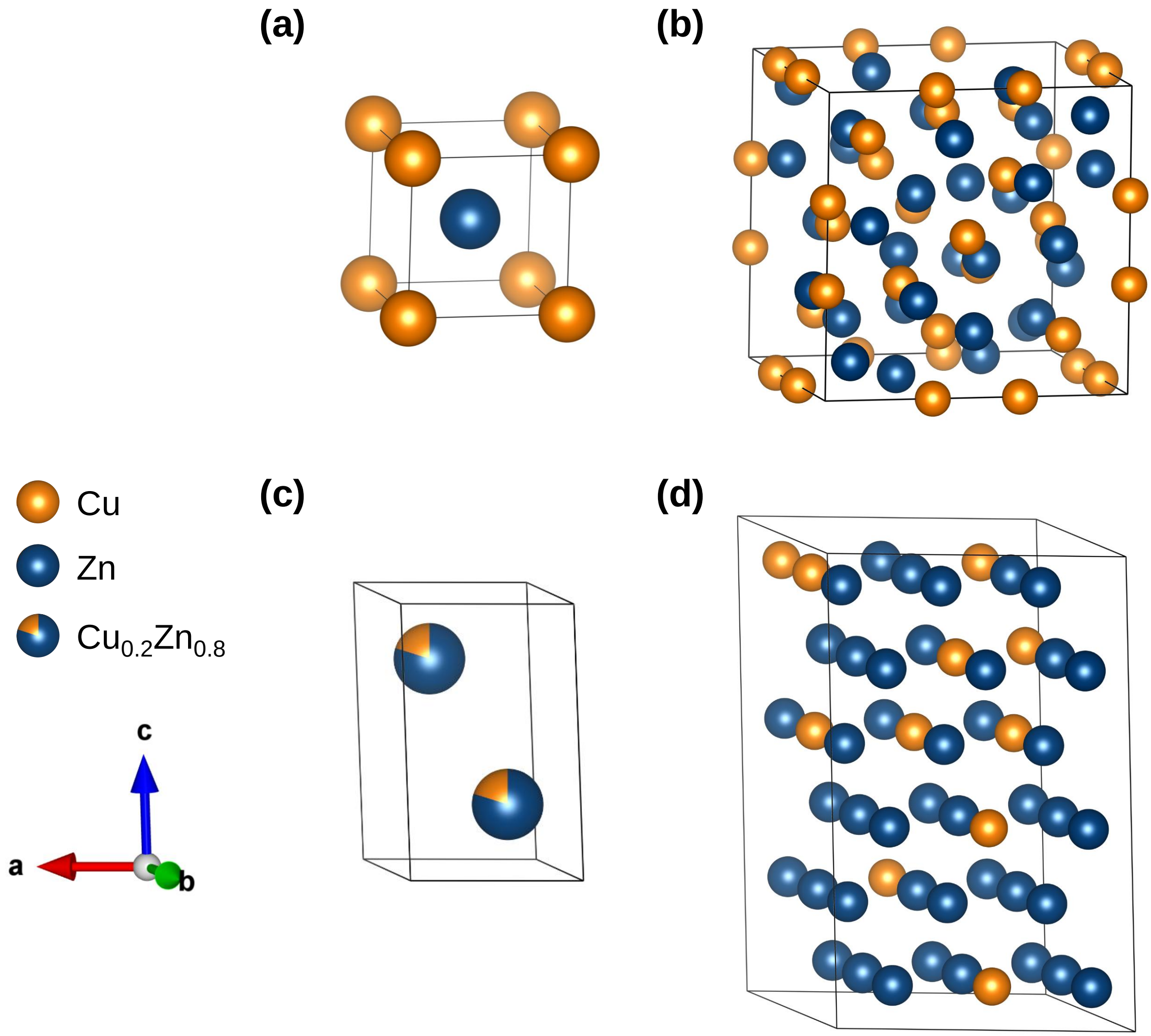

Fig.1 Elemental atom distribution of (a) CuZn, (b) Cu_5Zn_8 and $CuZn_4$ in (c) VCA model or (d) SQS (3×3×3 supercell) model before geometry optimization.

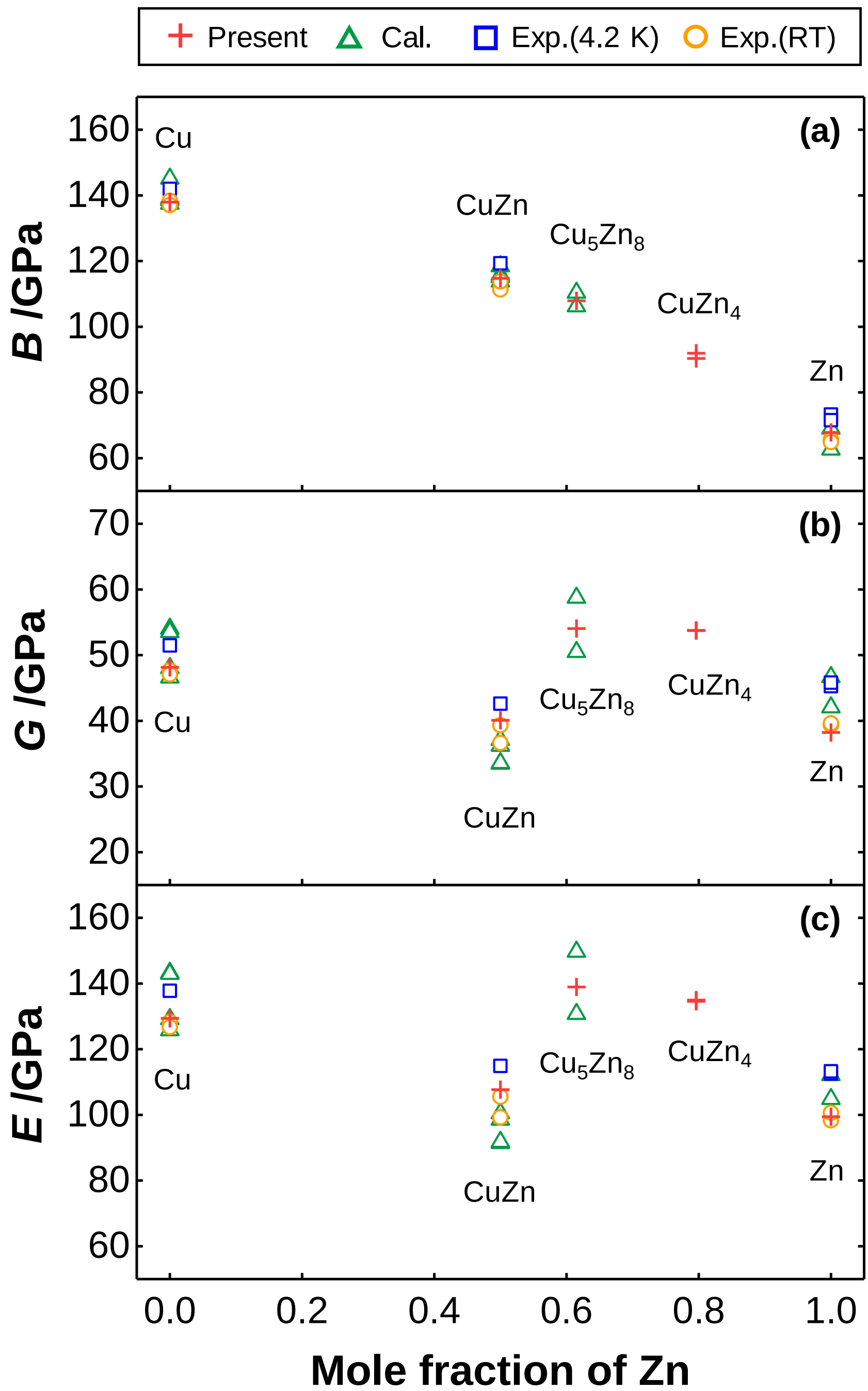

Fig.2 Mole fraction dependence of (a) bulk modulus B_H, (b) shear modulus G_H and (c) Young's modulus E_H of polycrystalline aggregate for Cu, CuZn, Cu_5Zn_8, $CuZn_4$ and Zn. The present calculation results in Hill model are compared with experimentally reported and previously computed values.

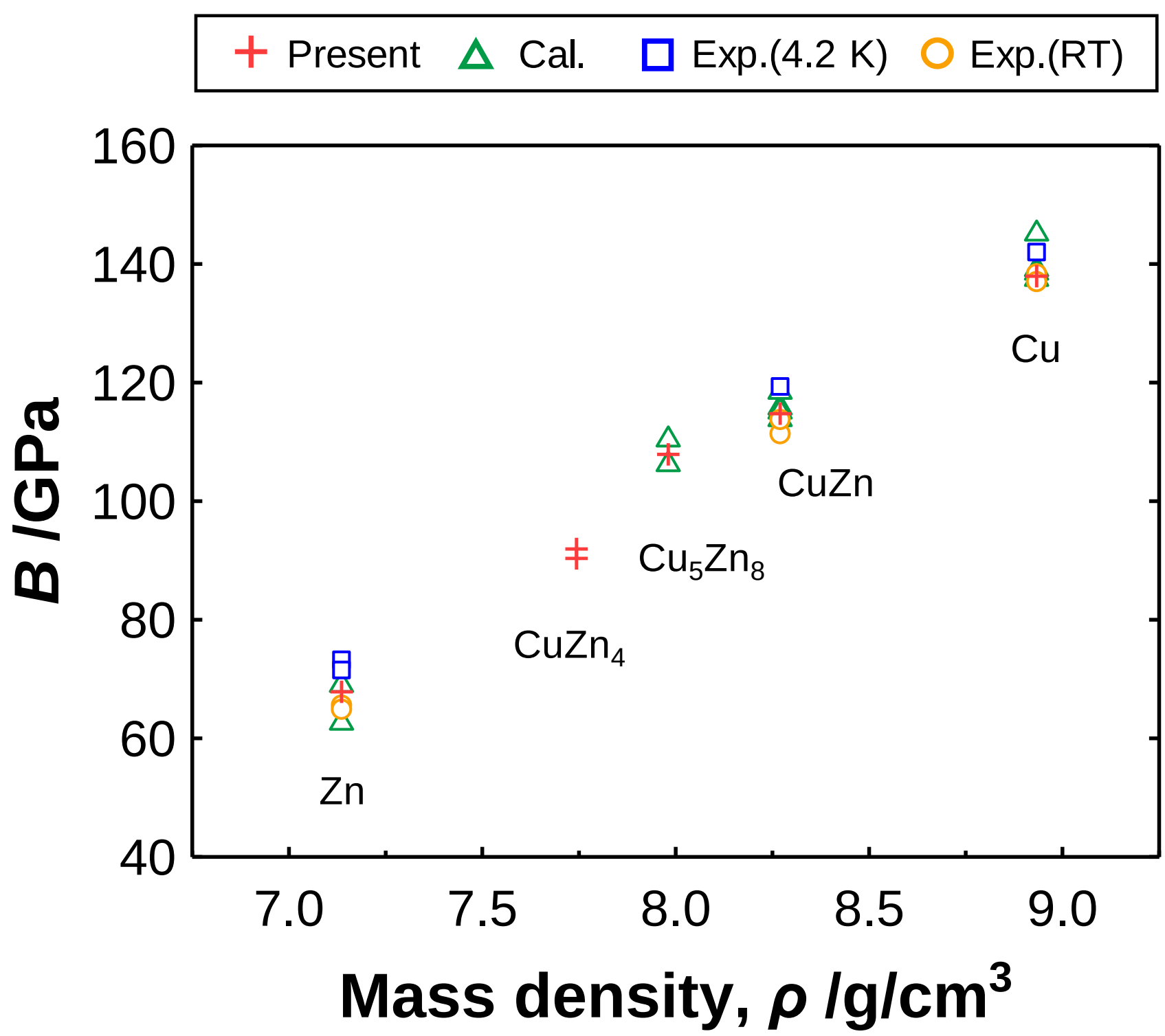

Fig.3 Mass density dependence of bulk modulus B_H of polycrystalline aggregate for Cu, CuZn, Cu_5Zn_8, $CuZn_4$ and Zn. The present calculation results in Hill model are compared with experimentally reported and previously computed values.

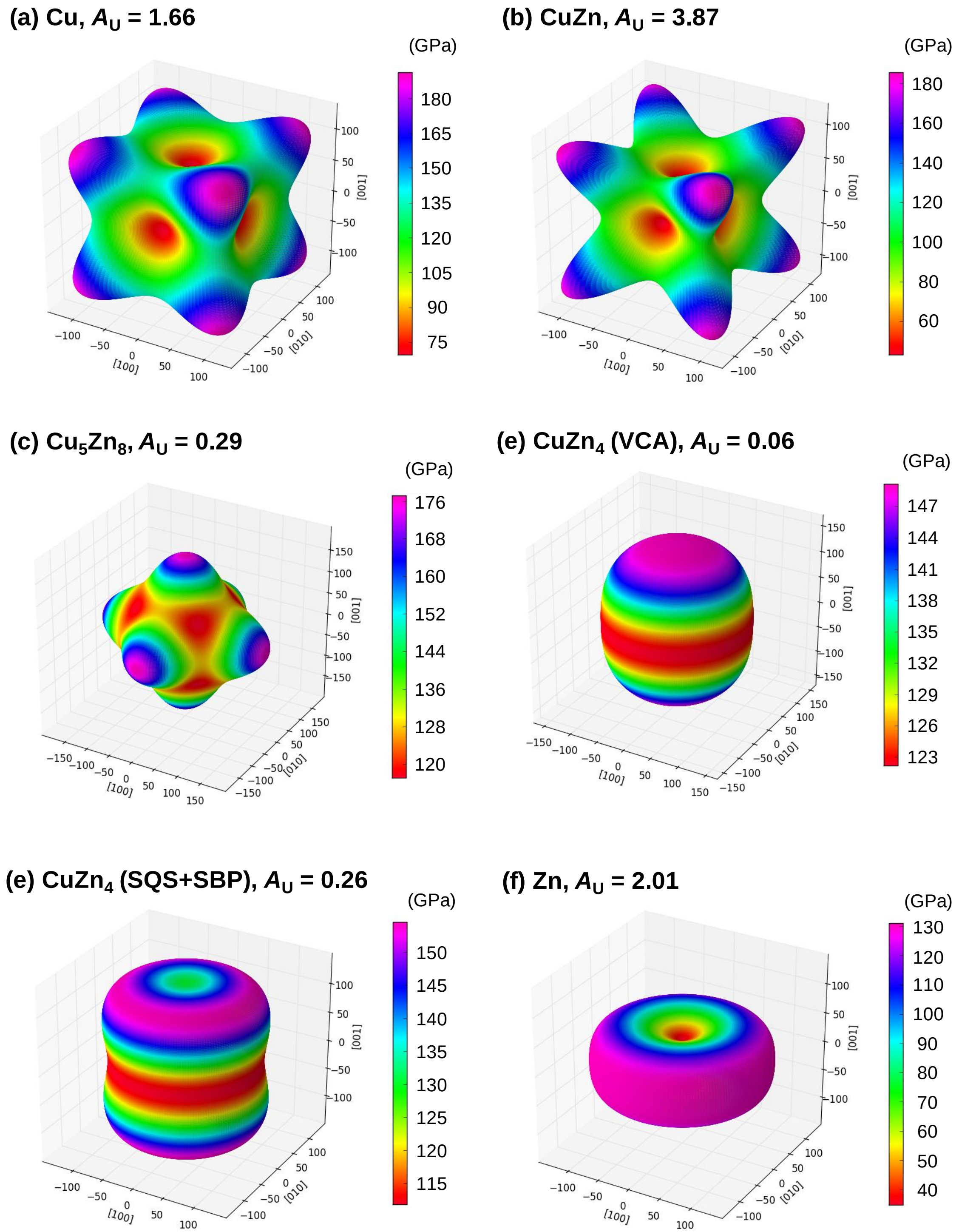

Fig.4 Directional anisotropy of Young's modulus E of single crystal for Cu, CuZn, Cu_5Zn_8, $CuZn_4$ and Zn. The magnitude of E in each direction is illustrated not only by color-coding according to each color scale but also by the distance from the center of the three-dimensional space.

Author Contributions Section

Conceptualization, H.I. and S.H.; Methodology, H.I. and S.H.; Investigation, H.I.; Writing – Original Draft, H.I.; Writing –Review & Editing, S.H.; Funding Acquisition, S.H.; Resources, S.H.; Supervision, S.H.

Credit Author Statement

Conceptualization, H.I. and S.H.; Methodology, H.I. and S.H.; Investigation, H.I.; Writing – Original Draft, H.I.; Writing –Review & Editing, S.H.; Funding Acquisition, S.H.; Resources, S.H.; Supervision, S.H.

*Declaration of Interest Statement

Declaration of interests

☒ The authors declare that they have no known competing financial interests or personal relationships that could have appeared to influence the work reported in this paper.

☐The authors declare the following financial interests/personal relationships which may be considered as potential competing interests: